AIMS Energy, 10(3): 535–552.
DOI: 10.3934/energy.2022027
Received: 03 April 2022
Revised: 14 June 2022
Accepted: 20 June 2022
Published: 23 June 2022

http://www.aimspress.com/journal/energy

Research article

BESS based voltage stability improvement enhancing the optimal control of real and reactive power compensation

Habibullah Fedayi[1,2,*], Mikaeel Ahmadi[1], Abdul Basir Faiq[2], Naomitsu Urasaki[1] and Tomonobu Senjyu[1]

[1] Graduate School of Engineering and Science, University of the Ryukyus, 903-0213 Nishihara, Okinawa, Japan
[2] Department of Electrical and Electronics, Faculty of Engineering, Kabul University, 1001, Jamal Mina, Kabul, Afghanistan

*** Correspondence:** Email: habibullahfedayi@gmail.com; Tel: +818088568421.

Abstract: With the increase in the integration of renewable energy resources in the grid and ongoing growth in load demand worldwide, existing transmission lines are operating near their loading limits which may experience voltage collapse in a small disturbance. System stability and security can be improved when the closeness of the system to collapse is known. In this research, voltage stability of IEEE 30 bus test network is analyzed and assessed under continuously increasing load condition, utilizing the Critical Boundary Index (CBI); and improved with continuous integration of battery energy storage system (BESS). BESS is considered to be a hybrid combination of storage units and voltage source converter to have a controllable real and reactive power output. Security constraint optimal power flow is utilized for optimally sizing the installed BESS. It is evident from the outcome of the research that the voltage stability of the system is controlled to be above the acceptable range of 0.3 pu CBI in all lines and the system voltage is kept within the acceptable and constrained range of 0.9–1.1 pu.

Keywords: voltage stability; optimization; battery storage; transmission line; power control; genetic algorithm

1. Introduction

Global greenhouse gas emissions and renewable energy resources (RERs) are two different impact expressions at the intersection of global trends. The field of power system engineering, which primarily influences the maintenance of both phenomena' effects, is expected to play a significant role in balancing the socio-environmental status by combating environmental crises and improving power system performance [1]. Incorporating intermittent RERs like solar and wind into the power system has changed how generation, transmission, and distribution are planned and operated. As a result, a revolution in power system circumstances has emerged, focusing attention on presenting smart and optimal practices in order to achieve the goal of contribution in power system engineering [2,3]. BESS as complement to such intermittent energies are deployed to increase renewable energy penetration and use.

The ongoing growth in the world population, increasing living standards, tremendous technological developments, liberalization in the power industry, and modernization of the cities have caused a severe increase in the load demand around the world. The power system components, especially the transmission and generation facilities in most countries, are either insufficient to supply the required demand or are outdated. Thus, many existing power networks worldwide are operating near their voltage stability margins. The ability of power systems to maintain a satisfactory voltage range at all buses under all power system operating conditions is referred to as voltage stability. Due to insufficient capacity to provide reactive power support at local load points, many power systems are at risk of voltage instability [4].

In the other words, voltage stability has been defined as the stable operation of the power system and its ability to maintain acceptable voltage in all buses, both during normal operation and when subjected to a fault or disturbance [5]. The growth in the deployment of renewable energy resources in the power systems increases the uncertainty of the power system. It causes disturbances and, as a result, raises the possibility of voltage instability [6]. Voltage instability is the case when the change in the load or generator dynamics causes an uncontrollable decline in voltage of one or all buses [7]. Voltage stability analysis is the study of power system response against the dynamics in load and generator units to maintain stable and reliable system operation [8]. The voltage stability of the system has been assessed through various mathematical formulations known as voltage stability indices [9–12]. Voltage stability indices describe the voltage stability condition of the system and how near the possibility of voltage collapse is; so that the operator can take preventive decisions.

Different indices and approaches have been used for the analysis of voltage stability. Some techniques analyze the P-V characteristic, which considers the relationship of voltage and active power in the transmission line. In contrast, some others consider the relationship of voltage and reactive power in transmission line as Q-V analysis [13,14]. Proposed stability analysis techniques and indices consider either the effect of real power change or reactive power change on voltage stability, while little work has been done related to the impact of both real and reactive power change on voltage stability analysis. A novel stability analysis technique and index called Critical Boundary Index (CBI) has been proposed in [15], which directly estimates the distance of operating point to the instability. Voltage stability analysis techniques are vital tools for the secure operation of the power system and help the planners take preventive measures and controls for stable system operation.

In the literature different voltage stability improvement techniques have been proposed for voltage stability improvement and voltage profile enhancement. Various methods of voltage stability

improvement techniques, as well as their merits and demerits are reviewed in [16]. In [17] different approaches for real time voltage stability margin control enhancing the reactive power reserve sensitivities were provided. The application and control of flexible alternating current transmission systems (FACTS) devices for voltage stability of power systems with high penetration of renewable energy resources is reviewed in [18]. Pradeepa, et al., studied the voltage stability of distribution network and used Genetic Algorithm to allocate distributed generation and capacitor bank for overall loss minimization and voltage profile improvement [19]. Roselyn, et al., introduces a multi-objective fuzzy-based generator rescheduling approach using FACTs devices for voltage stability enhancement. Mainly, the researchers have focused on the outcome of reactive power compensation on voltage profile and voltage stability improvement [20].

In the literature, optimal power flow has been identified as a key tool for operation and planning of power systems, which can adjust the control variables to optimize the production and transport of energy while maintaining the technical, economic, and environmental constraints [21]. The author in [22], proposes a novel configuration of particle swarm optimization to solve large-scale reactive power dispatch. Naderi, et al., in [23] proposes a framework for cyberattacks which lead the smart distribution networks to under voltage and warns the operators to have preventive measures and a voltage secure smart system.

As mentioned in the literature, different researchers have had their contribution in the aspect of voltage stability from voltage stability assessment and analysis to voltage stability improvement techniques, but still more research needs to be done on the influence of battery energy storage systems and variable energy resources on voltage stability. In the literature either the effect of real or reactive power change is analyzed on the voltage stability improvement, while it is important to study the effect of both real and reactive power change on voltage stability. The studies in the literature have conducted the voltage stability improvement in a base loading condition rather than continuously changing condition which is the nature of energy consumption in all energy systems. Voltage stability improvement has been achieved with compensation of a certain capacity of real or mostly reactive power, both real and reactive power compensation with controllable output based on the system performance has not been considered so far.

The contribution of this research can be mentioned as follows:

- The index utilized in this research analyzes the consequence of both real and reactive power change on voltage stability.
- In this research the voltage stability of the system is analyzed under a continuously increasing load rather than specific loading condition.
- A combination of battery storage and voltage source converter is integrated in the system to have both real and reactive power compensation.
- In this research the outcome of BESS is controlled having into consideration the CBI angle which provides a clear insight on the significance of real and reactive power compensation on voltage stability improvement.

In this paper we consider CBI based optimal placement and power control of BESS for real and reactive power support in IEEE 30 bus test network for voltage stability improvement. Security constrained genetic algorithm is used to keep the voltage stability index value in the specified acceptable range.

2. Voltage stability analysis

Considering the 2-bus transmission network in Figure 1. $V_i \ and \ V_k$ are the voltage magnitudes in the sending end and receiving end voltages, and $\delta_i \ and \ \delta_k$ are the voltage angles in sending end and receiving end, respectively. The power flow equation of the network shown is as follows:

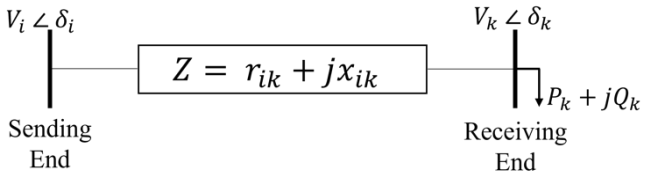

Figure 1. 2-Bus Transmission Line Model.

$$P_k + jQ_k = (V_k \angle \delta_k)\left(\frac{V_i \angle \delta_i - V_k \angle \delta_k}{r_{ik} + jx_{ik}}\right)^* \tag{1}$$

$$(P_k r_{ik} + x_{ik} Q_k) + j(P_k x_{ik} - r_{ik} Q_k) = V_i V_k \cos(\delta_i - \delta_k) - jV_i V_k \sin(\delta_i - \delta_k) - {V_k}^2 \tag{2}$$

where, $P_k \ and \ Q_k$ are the real and reactive power transferred to receiving end from sending end, and $r_{ik} \ and \ x_{ik}$ collectively are the transmission line impedance. The following equations can be derived out by separating the real and reactive parts of the above equation:

$$P_k \ r_{ik} + x_{ik} \ Q_k + {V_k}^2 = V_i \ V_k \ \cos(\delta_i - \delta_k) \tag{3}$$

$$P_k \ x_{ik} - r_{ik} \ Q_k = -V_i \ V_k \ \sin \ (\delta_i - \delta_k) \tag{4}$$

Adding the square of Eqs (3) and (4) we have (hint: $\sin^2(\delta) + \cos^2(\delta) = 1$):

$$(P_k \ r_{ik} + x_{ik} \ Q_k + {V_k}^2)^2 + (P_k \ x_{ik} - r_{ik} \ Q_k)^2 = {V_i}^2 \ {V_k}^2 \tag{5}$$

$$({V_k}^2)^2 + 2\left(P_k \ r_{ik} + x_{ik} \ Q_k - \frac{{V_i}^2}{2}\right){V_k}^2 + ({r_{ik}}^2 + {x_{ik}}^2) \ \left({P_k}^2 + {Q_k}^2\right) = 0 \tag{6}$$

Using the Pythagorean theorem, from Eq (6), $({V_k}^2)$ can be derived as:

$$\begin{aligned} {V_k}^2 = &-\left(P_k \ r_{ik} + x_{ik} \ Q_k - \frac{{V_i}^2}{2}\right) \\ &\pm \sqrt{\left(P_k \ r_{ik} + x_{ik} \ Q_k - \frac{{V_i}^2}{2}\right)^2 - ({r_{ik}}^2 + {x_{ik}}^2) \ \left({P_k}^2 + {Q_k}^2\right)} \end{aligned} \tag{7}$$

As both $V_i \ and \ V_k$ are positive, the discriminant of the subsequent equation above should be greater than or equal to zero. The state when the discriminant given in the equation below is equated to zero corresponds to maximum power transferable through the line for stable operation of the network, which we call the voltage stability margin of the specified line:

$$\sqrt{\left(P_k\ r_{ik} + x_{ik}\ Q_k - \frac{{V_i}^2}{2}\right)^2 - ({r_{ik}}^2 + {x_{ik}}^2)({P_k}^2 + {Q_k}^2)} = 0 \tag{8}$$

$$Q_k = \frac{\mp\sqrt{{x_{ik}}^2\ {V_i}^4 + {r_{ik}}^2\ {V_i}^4 - 4\ {x_{ik}}^2\ r_{ik}\ {V_i}^2\ P_k - 4\ {r_{ik}}^3\ {V_i}^2\ P_k}}{2\ {r_{ik}}^2} + \frac{2\ x_{ik}\ r_{ik}\ P_k - x_{ik}\ {V_i}^2}{2\ {r_{ik}}^2} \tag{9}$$

The voltage stability limit obtained from Eq (9) has been described in the (P, Q)—V characteristic shown in Figure 2, for different voltage levels V_i. The P-Q plane for a given specific voltage is shown in Figure 3, which shows the stable and unstable operating regions as well as the stability limit. The Coordinates of the point $C(X, Y)$ on the stability limit from the current operation point $K(P_0, Q_o)$ can be determined using the LaGrange multipliers. Where X and Y are the coordinates of the nearest point to the current operating point and are variables on the P-Q curve which should be calculated and P_0 and Q_o are the real and reactive power flow in the specific line under the current operating condition.

As $C(X, Y)$ is the stability curve:

$$C(X,Y) = \left(r_{ik}X + x_{ik}\ Y - \frac{{V_i}^2}{2}\right)^2 - ({r_{ik}}^2 + {x_{ik}}^2)\ (X^2 + Y^2) = 0 \tag{10}$$

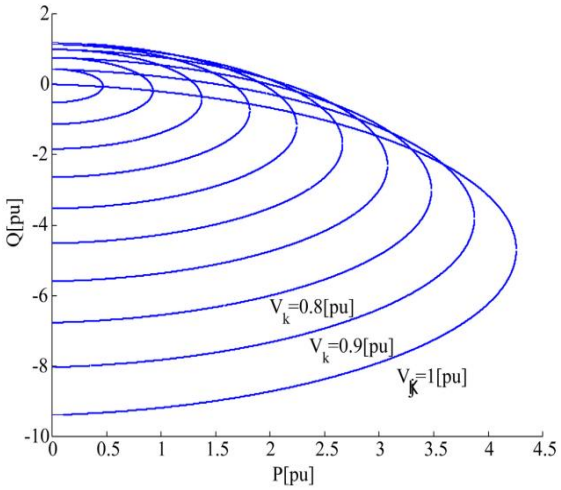

Figure 2. (P, Q)—V characteristic of line.

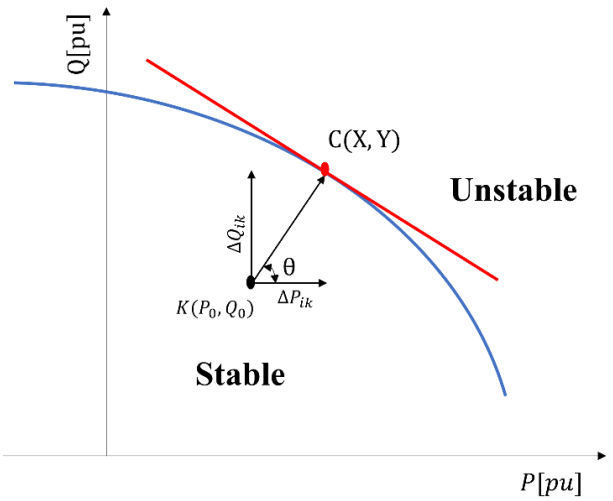

Figure 3. P—Q characteristic.

The shortest distance from the current operating point $K(P_0, Q_o)$, to the voltage collapse is a function of the coordinates of $C(X, Y)$. The minimum distance as shown in the Figure 3, is evaluated as follows:

$$f(X,Y) = \sqrt{(X-P_0)^2 + (Y-Q_0)^2} \;\; or \;\; simply \;\; f^2 = (X-P_0)^2 + (Y-Q_0)^2 \tag{11}$$

Using the LaGrange multiplier, following equation can be obtained:

$$F(X,Y,\lambda) = f^2(X,Y) - \lambda \;\; C(X,Y) \tag{12}$$

$$F(X,Y,\lambda) = \;\; (X-P_0)^2 + (Y-Q_0)^2 - \lambda\left(\left(r_{ik}X \;\; + \;\; x_{ik} \;\; Y - \frac{{V_i}^2}{2}\right)^2 - ({r_{ik}}^2 + {x_{ik}}^2) \;\; (X^2+Y^2)\right) \tag{13}$$

From partial differentiation of above equation with respect to X, Y and λ, following three independent equations are derived:

$$F_x = 2X \;\; - \;\; 2P_0 - \;\; \lambda\left(2\left(r_{ik}X + x_{ik}Y - \frac{{V_i}^2}{2}\right)r_{ik} - 2({r_{ik}}^2 + {x_{ik}}^2)X\right) = 0 \tag{14}$$

$$F_y = 2Y \;\; - \;\; 2Q_0 - \;\; \lambda\left(2\left(r_{ik}X + x_{ik}Y - \frac{{V_i}^2}{2}\right)x_{ik} - 2({r_{ik}}^2 + {x_{ik}}^2)Y\right) = 0 \tag{15}$$

$$f(X,Y) = \sqrt{(X-P_0)^2 + (Y-Q_0)^2} \;\; or \;\; simply \;\; f^2 = (X-P_0)^2 + (Y-Q_0)^2 \tag{16}$$

Coordinates of the nearest point (X, Y) of voltage collapse to the operating point can be evaluated by solving the Eqs (14), (15) and (16). The distance can be evaluated by the components of real and reactive power deviation as:

$$\Delta P_{ik} = X - \ P_0 \tag{17}$$

$$\Delta Q_{ik} = Y - \ Q_0 \tag{18}$$

Consequently, the Critical Boundary Index (CBI) is calculated as:

$$CBI_{ik} = \sqrt{\Delta P_{ik}{}^2 + \ \Delta Q_{ik}{}^2} \angle \theta_{ik} \tag{19}$$

From CBI, the proximity of voltage collapse can be directly seen; as the CBI magnitude approaches zero means that system is heading toward voltage instability. Two different values can be extracted from the vectoral value of CBI.

CBI magnitude helps to identify the stability status of the power system, while the phase angle θ_{ik} helps us determine the effect of real and reactive power increment as well as compensation on the stability:

$$\theta_{ik} = tan^{-1}\left(\frac{\Delta Q_{ik}}{\Delta P_{ik}}\right) \tag{20}$$

3. BESS modelling and control

3.1. BESS modelling and formulation

With high penetration of renewable energy resources in power systems, battery energy storage systems have been an important part of power systems. BESSs are the intermittent part of renewable energy sources in power system. BESSs can be an alternative for transmission and distribution network equipment upgrade and expansion due to increasing load demand and help as a source of energy during peak load and contingencies [24]. To provide both active and reactive power for the network, the BESS is considered as a hybrid combination of storage batteries and Voltage Source Converter (VSC). The apparent power injected to the bus from BESS can be controlled by VSC. The model of BESS and its current source equivalence is given in Figure 4. The battery current is given as a function of injected real and reactive power as well as bus voltage.

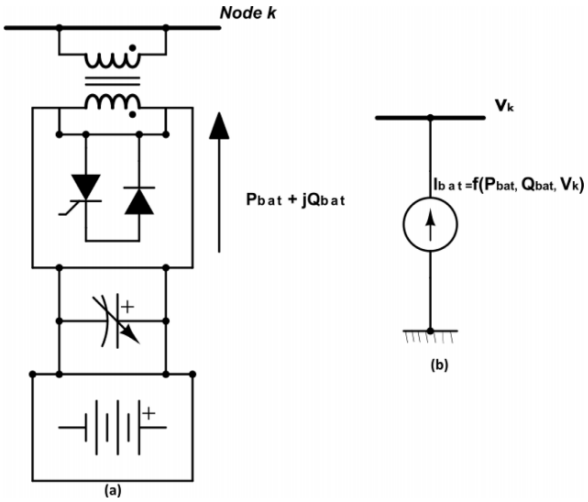

Figure 4. (a) VSC-BESS model and (b) BESS current injection equivalent model.

$$I_{bat} = \frac{P_{bat} - jQ_{bat}}{V_k \angle \delta_k} \tag{21}$$

where, I_{bat}, P_{bat} and Q_{bat} are the current exchange between BESS and grid, the real power injection from BESS to the grid and reactive power injection between BESS and the grid, respectively. The current constraint is determined by the converter rating (S_{BESS}^{max}) as:

$$I_{bat}^{max} = \frac{S_{BESS}^{max}}{V_k^{min}} \tag{22}$$

where V_k^{min}, is the lowest permissible and safe bus voltage where the BESS is integrated. The active and reactive power output of BESS can be controlled through the phase shift between the voltage and current of (VSC) inverter. If the current output of BESS is in phase with voltage, the BESS provides pure active power with the maximum active power compensation of:

$$P_{BESS}^{max} = S_{BESS}^{max} \tag{23}$$

While reactive power limit at every operating condition can be estimated as:

$$Q_{bat}(t) \leq \sqrt{S_{BESS}^{max\,2} - P_{bat}(t)^2} \equiv Q_{BESS}^{max} \tag{24}$$

3.2. BESS output power control mechanism

The consequence of BESS installation and its real and reactive power output control on stability margin improvement can be seen in the Figure 5.

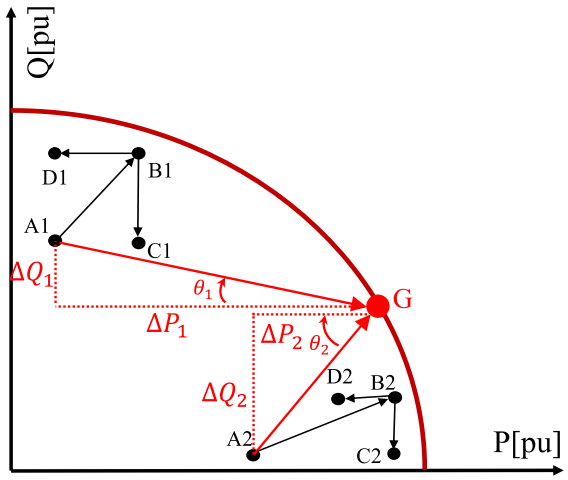

Figure 5. BESS compensation and its effect on voltage stability.

Voltage stability margin of a power system defines the distance of a power system to nearest voltage collapse point under specific condition. In Figure 5, three different operation points are considered, A1 and A2 are points far from the stability limit, while point G is located on the stability limit or voltage collapse point. Simultaneous increment in both real and reactive power transfer moves the operating points to the new operating conditions of B1 and B2, respectively, which are really close to the stability margin or voltage collapse point. In the case of B1, pure real power compensation shifts the operating point to the point D1, and pure reactive power compensation shifts the operating point to C1. Similarly, pure real power compensation in the B2 operating condition, shifts the operating point to D2 and pure reactive power compensation shifts to C2. As it can be seen, in the first operating condition (in B1 operating point), reactive power compensation has better effect on voltage stability improvement and in the second operating point, real power compensation provides better consequence on voltage stability.

Two triangles formed by the red hidden lines in Figure 5 shows the stability angle of operating points A1 and A2 referenced from a collapse point G which are θ_1, and θ_2 respectively. Having into consideration, the results in Figure 5, it can be inferred that the smaller the stability angle the more reactive power compensation is dominant for voltage stability improvement, contrarily, the bigger the stability angle is, the more dominant is the real power compensation on voltage stability improvement.

Thus, the angle θ, provides important insights regarding the real and reactive power output control of BESS for better voltage stability improvement and should be considered as the parameter for BESS output power controller.

4. Problem formulation

As described in section 3, BESS is integrated in the system in order to improve the voltage stability of the system. Thus, the apparent power output of the overall installed BESSs is minimized having the voltage stability and other power system components as system constraints. The effect of BESS can be clearly seen on the line voltage stability index (CBI) value, phase angle (θ_{lk}), and the bus voltages.

4.1. Objective function

In this work BESS is considered to be installed in three different buses considered to be the most crucial buses for compensation and the most suitable location for transmission line stability improvement. The objective in the system is the minimization of apparent power output of BESSs, as a result the minimization of the cost for this compensation. The optimal size is achieved by genetic algorithm optimization. Optimization is done for a continuously increasing load power system and the optimal size is determined for different loading conditions. The objective function is the minimum total apparent power of all BESSs.

$$\text{Min:} \quad T_{BESS} = \sum_{x=1}^{n_{bat}} S_{BESS_x} \ (\sigma) \tag{25}$$

$$S_{BESS_s} = \sqrt{{P_{BESS_x}}^2 + {Q_{BESS_x}}^2} \tag{26}$$

While n_{bat}, σ, S_{BESS_s}, P_{BESS_x}, Q_{BESS_x}, and T_{BESS} are total number of battery storages installed, the load increment step, the apparent power injected by BESS at the selected buses, the real power injected by BESS at the selected buses, the reactive power injected by BESS at the selected buses and the total of all installed BESSs apparent powers, respectively.

4.2. System constraints

Following power system constraints and voltage stability constraints are considered in the system.

4.2.1. Equality constraints:

$$P_{gl} + P_{dl} - \sum_{k=1,k\neq l}^{n_{tl}} P_{lk} + P_{bat_x} \tag{27}$$

$$Q_{gl} + Q_{dl} - \sum_{k=1,k\neq l}^{n_{tl}} Q_{lk} + Q_{bat_x} \tag{28}$$

4.2.2. Inequality constraints:

$$P_g^{min} \leq P_{gl} \leq P_g^{max} \tag{29}$$

$$Q_g^{min} \leq Q_{gl} \leq Q_g^{max} \tag{30}$$

$$V^{min} \leq V_l \leq V^{max} \tag{31}$$

$$\left|S_{L_{lk}}\right| \leq S_{L_{lk}}^{max} \tag{32}$$

$$CBI_{lk} \geq 0.3 \qquad \forall_{l,k} \in n_b \tag{33}$$

$$0 \leq P_{bat_x} \leq P_{bat}^{max}; \qquad \forall_x \in n_{bat} \tag{34}$$

while n_{bat} and n_b are the number of batteries and buses, respectively.

5. Simulation

5.1. Simulation network and condition

IEEE 30 bus test system model is considered in this paper for the simulation and operation of the proposed voltage stability improvement technique. The IEEE 30 bus test system is a sub transmission network with 6 generation buses with a total of 300 MW and 151 MVAR real and reactive power generation respectively. The maximum BESS real power compensation is restricted to be 60 MW and the base power for the power flow calculations is assigned to be 100 MW in the current research. In order to have a better reflection of the BESS compensation on the voltage stability of the system, the overall load consumption of the system is incremented step wisely until voltage collapse occurs in the system or in other words, the critical boundary index value of at least one line in the system becomes very low and tends to approach zero. The load increment can be done according to the equations below:

$$P_{dl\ new} = P_{dl} * \sigma \tag{35}$$

$$Q_{dl\ new} = Q_{dl} * \sigma \tag{36}$$

In order to identify the best location buses for BESS allocation, the line stability index values are ranked in a loading condition above the base loading level using CBI. At the specified loading condition, the weakest lines from voltage stability perspective are ranked as below:

Table 1. Critical lines ranking near collapse, according to CBI value.

Rank	Line Number	CBI [pu]
1	38	0.0690
2	39	0.1549
3	37	0.1760
4	36	0.1768
5	12	0.1858
6	34	0.1997
7	2	0.3141
8	33	0.3990
9	5	0.4133
10	15	0.4453

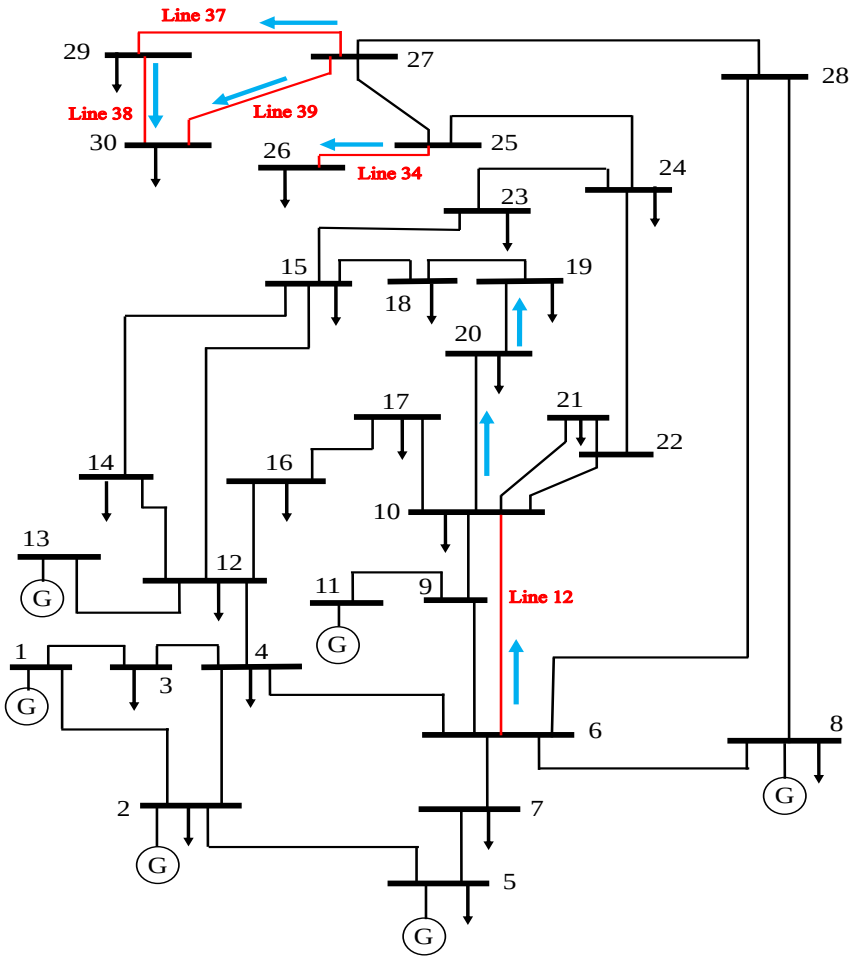

Figure 6. IEEE 30 bus test network with critical lines and their power flow direction.

As shown in the Table 1, the weakest lines are 38, 39, 37, 36, 12 and 34 and so on, while lines 38 and 39 are mutually linked to the bus number 30, and lines 36 and 37 are linked to bus 27 which is again directly linked to bus 30. Line 34 connects buses 25 and 26, while the bus 26 has higher load consumption and does not have link to any other bus. Line 33 is again connected to bus number 25. The other weaker line is line number 12 which links buses 6 and 10. As it can be seen from the Figure 6, line 12 is the line that delivers a high percentage of load to bus 10 and from bus 10 to other load buses, where bus 19 is the main consumer of both real and reactive power in its vicinity. The blue arrows in Figure 6 show the power flow direction in the most critical lines and this significantly drops the number of candidate locations for BESS compensation. Having the CBI values of critical lines, the installed loads in the load buses (which can be seen in the network bus data provided in the Appendices), and power flow direction in the critical lines, identifies buses 30, 26, and 19 as most suitable buses for BESS compensation.

5.2. Simulation results and discussion

As described in the above section, buses 30, 26, and 19 are selected to be the best locations for BESS installation. The simulation is carried out in two different scenarios. In the first scenario, the

voltage stability condition and voltage variation of the system is monitored in a continuously increasing load condition. In the second scenario, the system load is continuously increased while optimally controlling the real and reactive power compensation of the BESS output simultaneously.

The simulation results for the first scenario are illustrated in the Figures 7–9. Figure 7 shows the line stability index values for a continuously increasing load. As mentioned in the previous sections, CBI value shows the closeness of the line to voltage collapse and reaches the collapse at 0 pu. As shown in Figure 7, the critical lines are identified to be lines 36–39, 12, and 34 and are all below the acceptable threshold CBI value. At the load increment of 190%, the voltage collapse occurs, and at this stage the line stability index values are shown in Table 1.

Figure 8 illustrates the voltage stability angle for the critical lines which distinguishes whether real or reactive power compensation has better consequence on voltage stability improvement. As shown in the Figure 8, stability margin angle drops significantly in all lines as system load increases.

System bus voltages are shown in Figure 9, for continuously increasing load while not having BESS compensation. The voltage in this system is constrained to be within 0.9–1.1 pu, but as shown in the Figure 9, the first bus that passes beyond the minimum acceptable voltage range is bus 30, and the second bus passing below threshold voltage is bus 26. Following bus 26 are buses 29, 24, 25, and 19. Figure 9 is a good proof for the validity of candidate locations for BESS compensation that are buses 30, 26, and 19. Bus 30 will also improve the voltage profile of bus 29 which are directly linked. Bus 26 improves the voltage profile buses 24 and 25 as are in the vicinity of each other; finally, the other candidate bus is bus 19 both from voltage profile point of view and line stability magnitude point of view.

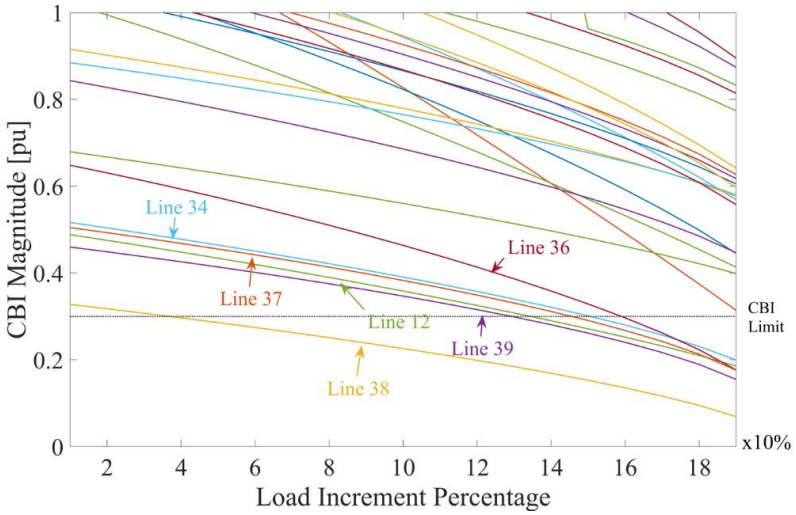

Figure 7. CBI magnitude for continuously increasing system load without BESS compensation.

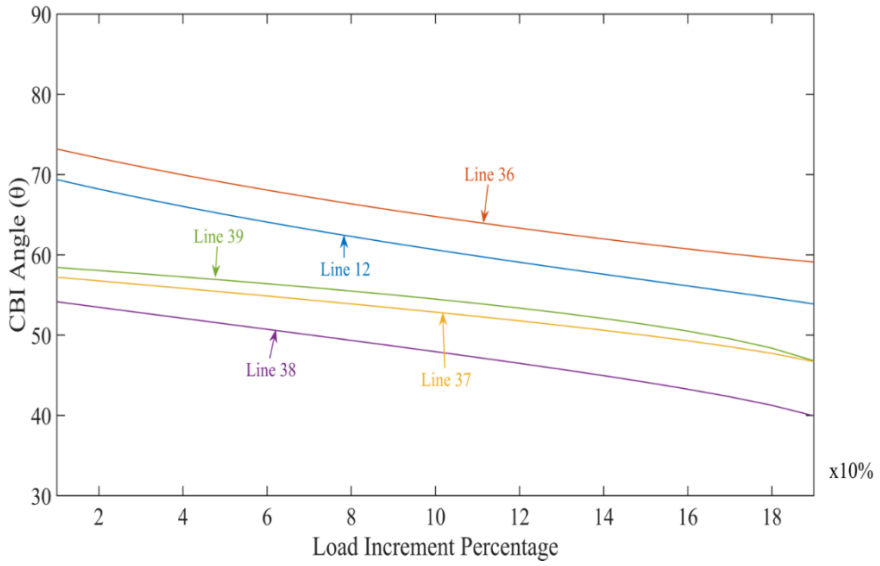

Figure 8. CBI angle for continuously increasing load without BESS compensation.

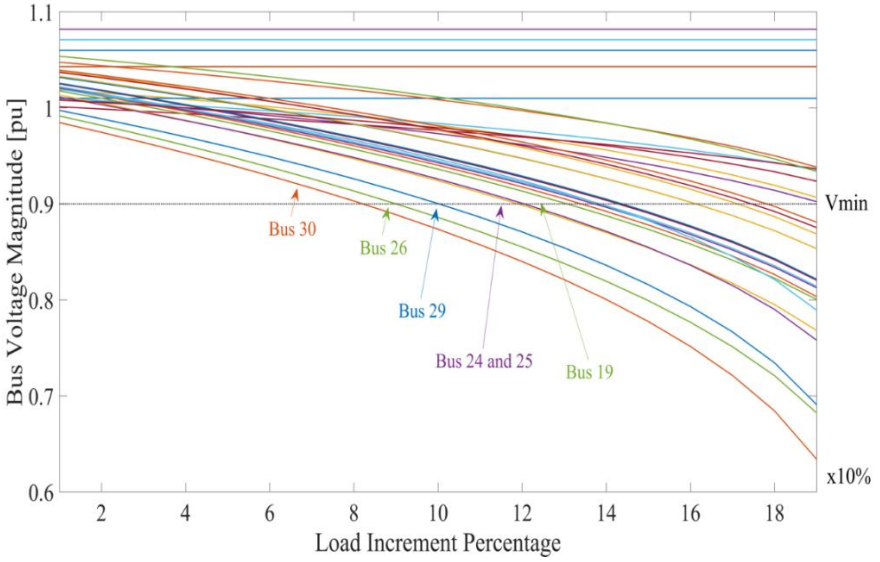

Figure 9. Bus voltage magnitude for continuously increasing load without BESS compensation.

Figures 10–12, illustrate the simulation results for the second scenario, while system load is continuously increased with simultaneously increasing the optimal real and reactive power output of BESSs. As shown in Figure 10, the CBI magnitude of lines are all above the acceptable CBI limit of 0.3 pu. The critical lines that all passed below the CBI limit are again identified and are shown to be above the CBI limit.

Figure 11 shows the system voltage for continuously increasing load, while having BESS compensation in 3 specified locations. It was obvious from the Figure 9 that even before voltage collapse, the voltage magnitude in many buses decrease below the acceptable voltage limit. In this case, the voltage collapse may not occur, but power gains the steady state operation in a voltage level

that is not acceptable. Figure 10 shows that with optimal control of BESS integration, all buses operate in a secure voltage level.

Figure 12 shows the stability margin angle or CBI angle for the second scenario. As it was obvious that with load increment the stability angle or CBI angle decreased significantly with increasing load, which means more reactive power compensation is required for stability improvement which is not good for inverter operation of BESS. But with optimally controlling the real and reactive power output of BESS, the stability angles of the critical lines have improved in Figure 12 which somehow stabilizes the effect of both real and reactive power on voltage stability improvement.

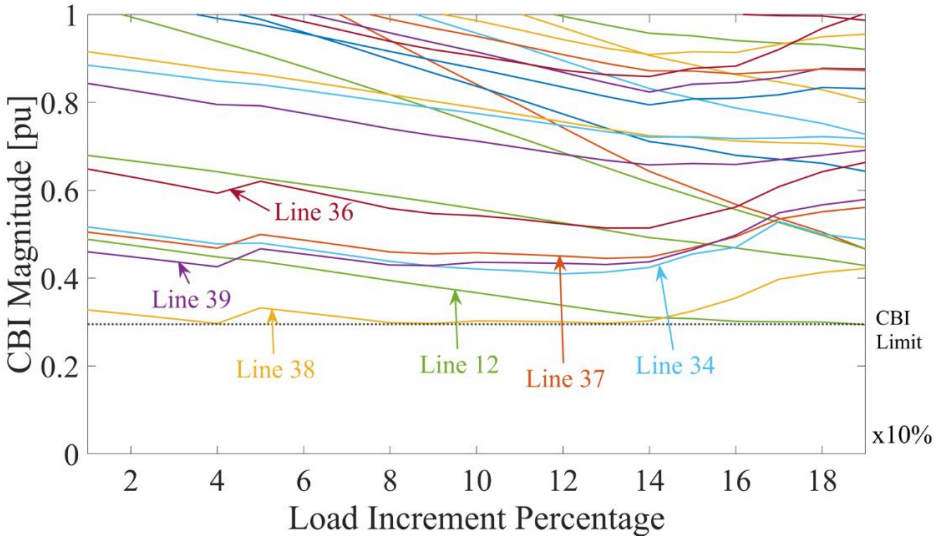

Figure 10. CBI magnitude for continuously increasing load with BESS.

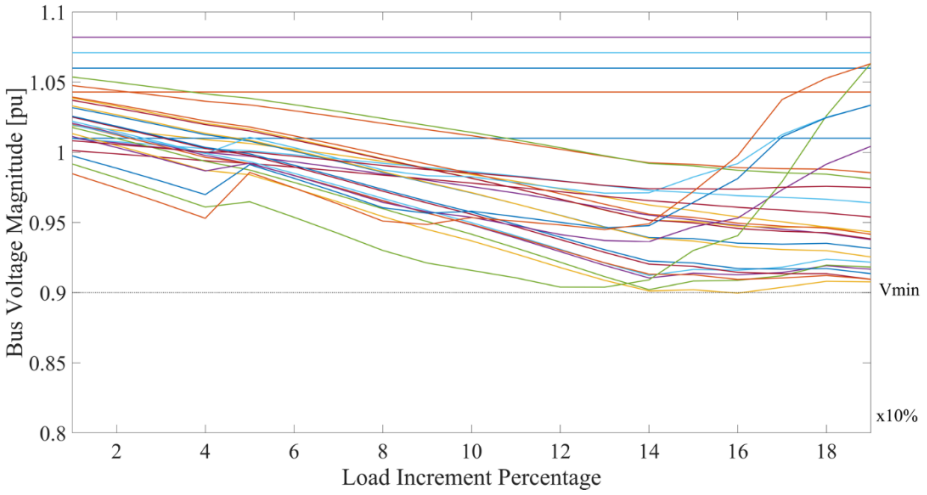

Figure 11. Bus voltage magnitude for continuously increasing load with BESS.

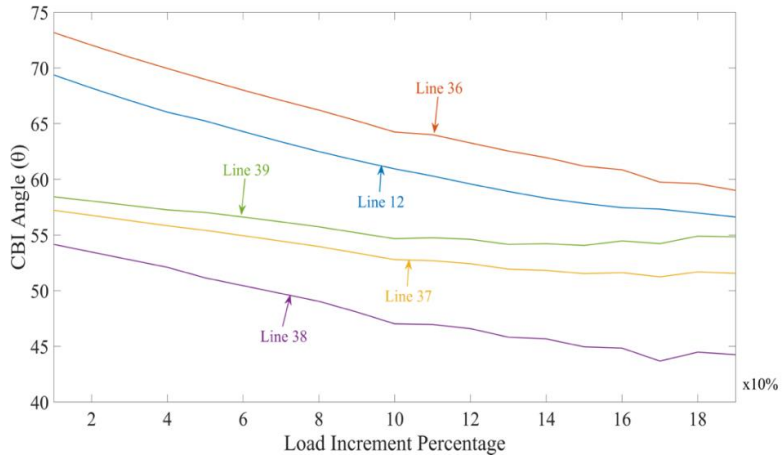

Figure 12. CBI angle for continuously increasing load with BESS.

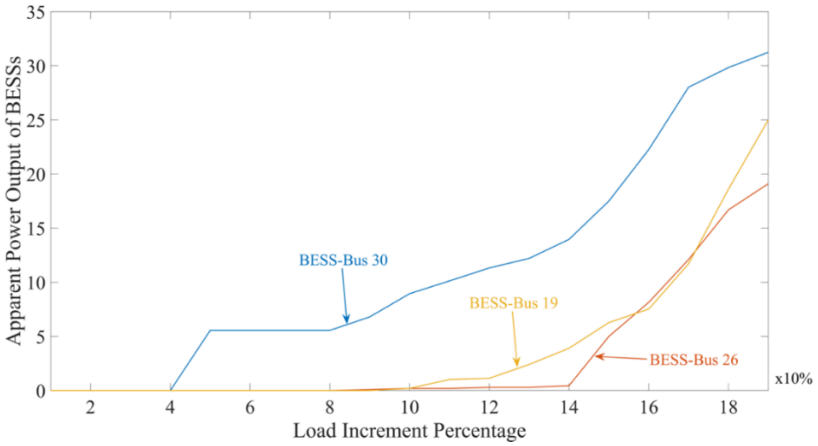

Figure 13. Apparent power output of three BESSs with increasing load.

Finally, the Figure 13, shows the apparent power output of all three BESSs for different loading levels.

6. Conclusions

As voltage has been one of the major incidents causing the voltage collapse and blackouts, it is worth to have a system secure from the voltage stability point of view which is less prone to voltage collapse. In this research article, the voltage stability of continuously increasing load system is analyzed and optimally improved utilizing the optimal control of real and reactive power output of BESS. The results in Figures 10–12 clearly indicates the significance of the proposed method as both the stability index value is with the constrained range of higher than 0.3 pu and the voltage pu in all buses is within the acceptable range of 0.9–1.1 pu. As expected from Figures 8 and 10 which prove that the weakest line is line 30 and the lines in the vicinity of line 30, which requires a higher amount of BESS compensation. It is concluded that a combination of real and reactive power compensation for voltage stability improvement is a significant and more effective way of voltage stability enhancement, and it is better to have a compensation unit which's output power can be controlled

depending on system requirements. As the future steps of research, the 24-hour operation of BESS for voltage stability improvement and peak load shaving will be considered having in to account the uncertainty of renewable energy integration in to energy systems.

Conflict of interest

The authors declare no conflict of interest.

References

1. Ahmadi M, Lotfy ME, Howlader AM, et al. (2019) Centralised multi-objective integration of wind farm and battery energy storage system in real-distribution network considering environmental, technical, and economic perspective. *IET Gener, Trans Distrib* 13: 5207–5217. https://doi.org/10.1049/iet-gtd.2018.6749
2. Ahmadi M, Lotfy ME, Danish MSS, et al. (2019) Optimal multi-configuration and allocation of SVR, capacitor, centralised wind farm, and energy storage system: a multi-objective approach in a real distribution network. *IET Renewable Power Gener* 13: 762–773. https://doi.org/10.1049/iet-rpg.2018.5057
3. Ahmadi M, Lotfy ME, Shigenobu R, et al. (2019) Optimal sizing of multiple renewable energy resources and PV inverter reactive power control encompassing environmental, technical, and economic issues. *IEEE Syst J* 13: 3026–3037. https://doi.org/10.1109/JSYST.2019.2918185
4. Ahmadi M, Adewuyi OB, Danish MSS, et al. (2021) Optimum coordination of centralized and distributed renewable power generation incorporating battery storage system into the electric distribution network. *Int J Electr Power Energy Syst* 125: 106458. https://doi.org/10.1016/j.ijepes.2020.106458
5. Taylor CW (1994) *Power System Voltage Stability,* 1st Ed., New York: McGraw-Hill, 273p.
6. Bode A, Shigenobu R, Ooya K, et al. (2019) Static voltage stability improvement with battery energy storage considering optimal control of active and reactive power injection. *J Electr Power Syst Res* 172: 303–313. https://doi.org/10.1016/j.epsr.2019.04.004
7. Canizares CA, De Souza AC, Quintana VH (1996) Comparison of performance indices for detection of proximity to voltage collapse. *IEEE Trans Power Syst* 11: 1441–1450. https://doi.org/10.1109/59.535685
8. Echavarren FM, Lobato E, Rouco L, et al. (2011) Formulation, computation and improvement of steady state security margins in power systems. *J Electr Power Energy Syst* 33: 340–346. https://doi.org/10.1016/j.ijepes.2010.08.031
9. Mariana K, Abdelrahman AK, Ahmaed HH, et al. (2017) Development and application of a new voltage stability index for on-line monitoring and shedding. *IEEE Trans Power Syst* 33: 1231–1241. https://doi.org/10.1109/TPWRS.2017.2722984
10. Sayed Ali Abbas K, Dong RS (2017) DG placement in loop distribution network with new voltage stability index and loss minimization condition-based planning approach under load growth. *Energies* 10: 1203. https://doi.org/10.3390/en10081203
11. Moghavvemi M, Omar F (1998) Technique for contingency monitoring and voltage collapse prediciton. *IEEE Proc-Gener Transm Distrib* 145: 634–640. https://doi.org/10.1049/ip-gtd:19982355

12. Veerasamy V, Wahab NIA, Ramachandran R, et al. (2021) Recurrent network-based power flow solution for voltage stability assessment and improvement with distributed energy sources. *Appl Energy* 302: 117524. https://doi.org/10.1016/j.apenergy.2021.117524
13. Vadivelu KR, Marutheswar GV (2014) Fast voltage stability index based optimal reactive power planning using differential evolution. *Electr Electron Eng: Int (ELELIJ)* 3: 51–60.
14. Jirjees MA, Al-Nimma DA, Al-Hafidh MS (2018) Voltage stability enhancement based on voltage stability indices using FACTS controllers. *In 2018 International Conference on Engineering Technology and their Applications (IICETA)*, *IEEE*, 141–145. https://doi.org/10.1109/IICETA.2018.8458094
15. Furukakoi M, Adewuyi OB, Danish MSS, et al. (2018) Critical Boundary Index (CBI) based on active and reactive power deviations. *Int J Electr Power Energy Syst* 100: 50–57. https://doi.org/10.1016/j.ijepes.2018.02.010
16. Vanishree J, Ramesh V (2014) Voltage profile improvement in power systems-A review. *In 2014 International Conference on Advances in Electrical Engineering (ICAEE), IEEE*, 1–4. https://doi.org/10.1109/ICAEE.2014.6838533
17. Leonardi B, Ajjarapu V (2012) An approach for real time voltage stability margin control via reactive power reserve sensitivities. *IEEE Trans Power Syst* 28: 615–625. https://doi.org/10.1109/TPWRS.2012.2212253
18. Adetokun BB, Muriithi CM (2021) Application and control of flexible alternating current transmission system devices for voltage stability enhancement of renewable-integrated power grid: A comprehensive review. *Heliyon* 7: e06461. https://doi.org/10.1016/j.heliyon.2021.e06461
19. Pradeepa H, Ananthapadmanabha T, SandhyaRani DN, et al. (2015) Optimal allocation of combined DG and capacitor units for voltage stability enhancement. *Procedia Technol* 21: 216–223. https://doi.org/10.1016/j.protcy.2015.10.091
20. Roselyn JP, Devaraj D, Dash SS (2014) Multi-Objective Genetic Algorithm for voltage stability enhancement using rescheduling and FACTS devices. *Ain Shams Eng J* 5: 789–801. https://doi.org/10.1016/j.asej.2014.04.004
21. Naderi E, Narimani H, Fathi M, et al. (2017) A novel fuzzy adaptive configuration of particle swarm optimization to solve large-scale optimal reactive power dispatch. *Appl Soft Comput* 53: 441–456. https://doi.org/10.1016/j.asoc.2017.01.012
22. Naderi E, Pourakbari-Kasmaei M, Cerna FV, et al. (2021) A novel hybrid self-adaptive heuristic algorithm to handle single-and multi-objective optimal power flow problems. *Int J Electr Power Energy Syst* 125: 106492. https://doi.org/10.1016/j.ijepes.2020.106492
23. Naderi E, Pazouki S, Asrari A (2021) A region-based framework for cyberattacks leading to undervoltage in smart distribution systems. *In 2021 IEEE Power and Energy Conference at Illinois (PECI), IEEE*, 1–7. https://doi.org/10.1109/PECI51586.2021.9435216
24. Kawabe K, Yokoyama A (2014) Improvement of transient stability and short-term voltage stability by rapid control of batteries on EHV network in power systems. *Electr Eng Jpn* 188: 1–10. https://doi.org/10.1002/eej.22547

AIMS Press